IOP Publishing Plasma Physics and Controlled Fusion
Plasma Phys. Control. Fusion **63** (2021) 125005 (14pp) https://doi.org/10.1088/1361-6587/ac2cd8

Microturbulence in edge of a tokamak plasma with medium density and steep temperature gradient

Jingchun Li[1,*], Zhihong Lin[2], Jiaqi Dong[3], Huasheng Xie[4,6] and Songfen Liu[5]

[1] Department of Earth and Space Sciences, Southern University of Science and Technology, Shenzhen 518055, Guangdong, People's Republic of China
[2] University of California, Irvine, CA 92697, United States of America
[3] Southwestern Institute of Physics, Chengdu 610041, People's Republic of China
[4] Hebei Key Laboratory of Compact Fusion, Langfang, 065001, People's Republic of China
[5] School of Physics, Nankai University, Tianjin 300071, People's Republic of China
[6] ENN Science and Technology Development Co., Ltd., Langfang 065001, China

E-mail: jingchunli@pku.edu.cn

Received 23 April 2021, revised 4 August 2021
Accepted for publication 5 October 2021
Published 8 November 2021

Abstract

Gyrokinetic simulations of electrostatic micro-turbulence have been carried out for transport barriers (TBs) in tokamak plasmas. It is found that the ion temperature gradient (ITG) mode is dominant in the pedestal with medium density gradient and steep temperature gradient. The mode width shrinks with increase of the ratio of the density and temperature gradients, which is in good agreement with the analytic theory. Unstable mode with herringbone-like structure is excited in the simulation annulus. The simulation results also indicate that multiple ITG modes are induced by a high temperature gradient. Radial electric field shear decreases the mode growth rate while increases the real frequency. Finally, the generation of the GAM and its interaction with the turbulence are also observed in the nonlinear simulation.

Keywords: microturbulence, ion temperature gradient mode, I-mode, plasma confinement, tokamak

(Some figures may appear in colour only in the online journal)

1. Introduction

It is well accepted that anomalous cross-field particle, energy, and momentum transports are due to microturbulence excited by drift wave instabilities [1]. Ion temperature gradient (ITG) driven instability is one of the drift waves and is considered as a major factor for ion-scale turbulent transports. The microturbulence involves a very important and unexplained phenomenon in tokamak fusion plasmas: the transition from low (L) to high (H) confinement modes, where H-mode [2] has significantly better confinement property than that of the L-mode. It is crucial to understand the underlying physics mechanism, which largely depends on different types of instabilities that drive the turbulence. Therefore, the ITG mode has a significant effect on the transport transition and energy confinement [3–7].

The ITG modes have been intensively studied theoretically and experimentally. Some earlier work by Hatch and colleagues examined the physics of subdominant & coexisting modes [8]. A hierarchy of damped modes is found in the nonlinear turbulent state, which defines a potent energy sink and leads to saturation of turbulence [9]. However, most previous studies [10–13] at present mainly focused on modes in L-mode or H-mode plasma. For instance, Fulton *et al* [14] and Xie *et al* [15, 16] have studied the microturbulence for strong gradient (H-mode), using global gyrokinetic simulations, and found that the most unstable mode was not the ground eigenstate and the mode structure becomes unconventional. Additionally, Watanabe *et al* [17] have shown with the GKV code simulation

* Author to whom any correspondence should be addressed.

that the ITG turbulent transport in the inward-shifted operational mode in LHD stellarator, which features a larger growth rate of the ITG instability, is regulated by the zonal flows to a level comparable to the standard operational mode. Chang *et al* [18] have studied the ITG turbulence across an entire L-mode-like edge density pedestal in tokamak divertor plasma with a full-f gyrokinetic particle-in-cell code, XGC1, and their results indicate that a localized estimate of the ITG-driven thermal conductivity is not valid in an L-mode-type density slope. Singh *et al* [19] have also presented the effects of finite ballooning angles on linear ion temperature gradient driven mode using the GENE code.

In experiments, a new energy confinement mode (I-mode) in a stationary edge pedestal has been observed on the Alcator C-Mod [20]. The I-mode is characterized by an ordinary density gradient but a large temperature gradient. Experiments on the Alcator C-mod have achieved I-mode with 4MW ICRF, that is, the realization of I-mode under a high-power discharge [21]. The behavior of microturbulence in this confinement mode is still poorly understood. Recently, the results in the ASDEX Upgrade showed that the power threshold for triggering I-mode is independent of the heating method, and the L-I transition seems to be mainly determined by the edge pressure gradient [22]. The I-mode operation has also been confirmed in EAST, and the results show a deeper edge E_{r} well in the I-mode than that in the L-mode [23].

Theoretically, verification comparisons are performed for L-mode and I-mode plasma conditions in Alcator C-Mod with GENE and GYRO, and it is found that the two gyrokinetic codes' linear growth rates and real frequencies are in good agreement, but the heat fluxes are much different, and the rotation effects can explain part of this difference [24]. The modelling of an ASDEX Upgrade I-mode discharge via linear and nonlinear gyrokinetic simulations have also been carried with the GENE code [25]. Recently, GTC simulations find that a weekly coherent mode (WCM) can drive heat and particle transport close to the experimental levels in the I-mode experiments [26]. Since I-mode has the feature of high energy confinement but low particle confinement, it is beneficial to fusion in the following three aspects: one is to avoid the accumulation of impurities and He 'ash', and the other is to control the density more easily, the third is that the I-mode is generally stable to edge local mode (ELM), thus avoiding transient heat pulses that are expected to affect the lifetime of the divertor. Because I-mode has characteristics that L-mode and H-mode do not have, it may become a mode commonly used in fusion devices in the future, and theoretical and simulation research on this mode, including drift waves and turbulence in I-mode are rare. Therefore, it is necessary to conduct a thorough and systematic study of the turbulence characteristics in this mode. We use the HL-2A configuration here. Since I-mode has not yet been achieved on the HL-2A, we will decrease the density gradient based on H-mode according to the I-mode discharge characteristics. In the following contents, we call this type of plasma I-mode-like plasma/configuration, which is with medium density and steep temperature gradient.

In this work, we use the gyrokinetic toroidal code (GTC) [27, 28] to study the properties of electrostatic instabilities in transport barriers (TBs) of the I-mode-like plasmas. Our first principle gyrokinetic simulations find that the ITG modes are dominant in the pedestal of I-mode plasmas. The growth rate of ITG mode increases and its mode structure becomes narrower with increasing of toroidal mode number. It is shown for the first time that the ITG instability with a herringbone-like mode structure can be excited in an I-mode-like plasma, and the mode width shrink by increasing the ratio between the gradients of density and temperature. The underlying physics is also explained which has significant implications for turbulent transport.

The remainder of this paper is organized as follows. The gyrokinetic equation and physical model are introduced in section 2. The numerical results of ITG modes in I-mode-like plasmas are presented and analyzed in section 3. Finally, brief conclusions are drawn in section 4.

2. Model

The plasma is treated as a set of marker particles interacting with each other through self-generated electromagnetic fields in GTC. All of the simulations presented in this paper are electrostatic. The gyrokinetic equations describing toroidal plasmas are formulated as follows [29]:

$$\frac{\mathrm{d}}{\mathrm{d}t}f_\alpha(\boldsymbol{X},\mu,v_\parallel,t)=\left(\frac{\partial}{\partial t}+\dot{\boldsymbol{X}}\cdot\nabla+\dot{v}_\parallel\frac{\partial}{\partial v_\parallel}\right)f_\alpha=0 \tag{1}$$

where

$$\dot{\boldsymbol{X}}=v_\parallel\frac{\boldsymbol{B}}{B_0}+\boldsymbol{v}_{\mathrm{E}}+\boldsymbol{v}_{\mathrm{g}}+\boldsymbol{v}_{\mathrm{c}} \tag{2}$$

$$\dot{v}_\parallel=-\frac{1}{m_\alpha}\frac{\boldsymbol{B}^*}{B_0}\cdot(\mu\boldsymbol{\nabla}B_0+Z_\alpha\nabla\phi) \tag{3}$$

f_α is the distribution function in terms of gyro-center position $\boldsymbol{X}$, μ and $v_\parallel$ are the magnetic moment and parallel velocity of particle. Z_α and m_α are particle charge, and mass of a species α. B_0 is equilibrium magnetic field, $B=B_0+\delta B$, and $\delta B=0$ for electrostatic simulation, $\boldsymbol{b_0}=\boldsymbol{B}/B_0$ is the unit vector, and

$$\boldsymbol{B}^*=\boldsymbol{B_0}+\frac{B_0\,v_\parallel}{\Omega_\alpha}\boldsymbol{b_0}+\nabla B_0 \tag{4}$$

$\boldsymbol{v}_{\mathrm{E}}$, $\boldsymbol{v}_{\mathrm{c}}$, and $\boldsymbol{v}_{\mathrm{g}}$ are the $\boldsymbol{E}\times\boldsymbol{B}$ drift, magnetic curvature drift and grad-B drift velocities, respectively. They could be found in [29]. The electrostatic potential ϕ is calculated from solving gyrokinetic Poisson's equation [30]

$$\frac{4\pi Z_i^2\, n_i}{T_i}(\phi-\tilde{\phi}) = 4\pi(Z_i n_i - e n_e) \tag{5}$$

with

$$\tilde{\phi} = \frac{1}{2\pi}\int \phi(\boldsymbol{X}) f_{0i}(\boldsymbol{X},\mu,v_{\parallel})\delta(\boldsymbol{X}-x+\boldsymbol{\rho_i})d\boldsymbol{X}dv_{\parallel}d\sigma \tag{6}$$

where $\tilde{\phi}$ is the gyro-averaged potential, n_α is density, Ω_α is the cyclotron frequency. f_{0i} is the ion equilibrium gyrocenter distribution function, $\boldsymbol{\rho_i} \equiv -\boldsymbol{v_{i\perp}} \times \boldsymbol{b_0}/\Omega_i$ is the ion gyroradius vector, σ is the gyrophase angle. Collisions are included in some test cases but shown little influence on the general results. Therefore, the results in this paper no longer incorporate the collisionality, which means that we omit the collision operator in equation (1).

The gyrokinetic particle simulation uses the particle-in-cell (PIC) method to solve the gyrokinetic equation. To minimize the Monte-Carlo noise caused by the PIC method, the so-called δf scheme is adopted [31, 32]. We define $\delta f = f - f_0$, where f is the time-evolving distribution function of the system and f_0 is the equilibrium distribution function. The gyrokinetic equation (1) can then be rewritten so that $\delta f/f$ is now evolving in time rather than the full f [33]. This scheme greatly reduces the statistical fluctuations in the simulations. In order to ensure the accuracy and validity of the results, on the one hand, we conducted a convergence study on the number of grids and particles. We have guaranteed that the output results such as the growth rates can no longer be affected when the number of grids continues to increase. On the other hand, the GTC code has been benchmarked against the code such as XGC using full-f method, and the results with the fluid-kinetic hybrid electron model in GTC code are in agreement with simulation results with full-f method [34, 35], indicating that delta-f method is effective for exploring pedestal physics. A fluid-kinetic hybrid electron model [36, 37] which is based on the expansion of the electron response into adiabatic and non-adiabatic parts is used to efficiently treat electron dynamics. Therefore, some kinetic effects of electrons are retained in the simulations [38, 39]. It should be noted that the boundary conditions for electrostatic potential are zero at the radial boundary and periodic in poloidal and toroidal directions. This handling can guarantee all the turbulence-driving gradients at the boundaries go to zero smoothly [40].

3. Results

The HL-2A tokamak parameters are chosen in our simulation, i.e. the major radius $R_0 = 1.65$ m, the minor radius a $= 0.4$ m, the on-axis toroidal magnetic field $B_0 = 1.35T$, the plasma current is 180 kA, the density at the plasma core is $n_i = n_e = 2.0 \times 10^{19}$ m^{-3}, and the magnetic shear is defined as $s = (r/q)(dq/dr)$. $T_e(r) = T_i(r)$ and $n_e(r) = n_i(r)$. $L_n^{-1} = -dlnn/dr$, and $L_T^{-1} = -dlnT/dr$ are density and temperature gradient scale lengths, $\eta = L_n/L_T$ is the ratio of the density gradient scale length to the temperature gradient scale length. The q-profile $q(r) = 1.02 + r/a + (r/a)^2$ is used in the simulation. The geometry of HL-2A is chosen because we want to explore the features of I-mode on HL-2A before the I-mode experiment on it, so as to provide a certain reference and basis for the development of related experiments. The HL-2A discharge we are based on is a NBI heated and diverted plasma with an X-point, and it has a toroidal rotation. During the calculation, we artificially adjust the density gradient to make it consistent to the I-mode discharge parameters, ignore the possible change of beta and collisionality, and name this I-mode-like plasma. Our simulation with $R/L_T \approx 100$ and $\rho_i/L_T \approx 0.08$ satisfies the gyrokinetic assumption $\rho_i/L_T \ll 1$. The highest R/L_T we used in our simulation is 180, so we could still have the approximations: $\rho_i/L_T \ll 1$. Therefore, if R/L_T increases further, the standard nonlinear gyrokinetic ordering would become only barely justifiable. At these situations, one needs to use the model that based on the refined nonlinear gyrokinetic (NLGK) ordering for plasmas in transport barrier region [41, 42]. Figure 1 gives the equilibrium profiles we used. Since I-mode plasma characterised by the development of a H-mode temperature pedestal while the density remains roughly as in the L-mode, we set to $R_0/L_T = 100$, $R_0/L_n = 33$, the characteristic length of L-mode, I-mode-like, as well as H-mode are shown in table 1. Here $\eta = 3$, which is close to the η value in an I-mode plasma of ASDEX Upgrade. The simulation domain r is limited in the region from 0.7a to 1.0a. The radial position of peak gradient region is located at r/a $= 0.9$a.

We start the linear global gyrokinetic particle simulation with $n = 20$. The modes are found to be unstable for the above parameters in the edge plasma of HL-2A when we assume the electron response is adiabatic. The unstable modes still exist, and almost unchanged as the electrons are set to be non-adiabatic. Therefore, we can infer this mode as the ITG mode. Given in figure 2 are contour plots of the electrostatic potential of the ITG instability under L-mode (a1) (the parameters used here are the same as in figure 1 except that $R/L_T = R/L_n = 33$), I-mode-like (a2) $R/L_T = 100, R/L_n = 33$ and H-mode (a3) $R/L_T = 100, R/L_n = 100$ in a poloidal cross section, and the radial distributions of the Fourier components ((b1), (b2) and (b3), respectively) of the potentials $\delta\phi_m$ at $t = 5000t_0$, $t_0 = 0.002R_0/c_s$ is the time step size. Those mode structures are typically ballooning and peak at the low field side of the torus. Compared with the results in L-mode, herringbone-like radial mode structures appear unexpectedly, and clearly exists in the outboard region. The time history and the frequency spectra for the Fourier component ($n = 20$, $m = 54$) of the electrostatic potential in figure 2(a2) is shown in figure 3. We can see that two branches of the eigenmode coexist at the linear stage due to similar growth rates. The growth rate here is $3.3R_0/c_s$, and the two frequencies in Fourier spectrum are around $-0.8\omega_s$ and $-5.0\omega_s$, where the normalized frequency $\omega_s = 1/t_s = c_s/R_0$ and $c_s \equiv \sqrt{T_e/m_i}$. The ITG simulation shows that both branches have identified a conventional ballooning structure, localized around the mid-plane at the low field side (the ground eigenstate).

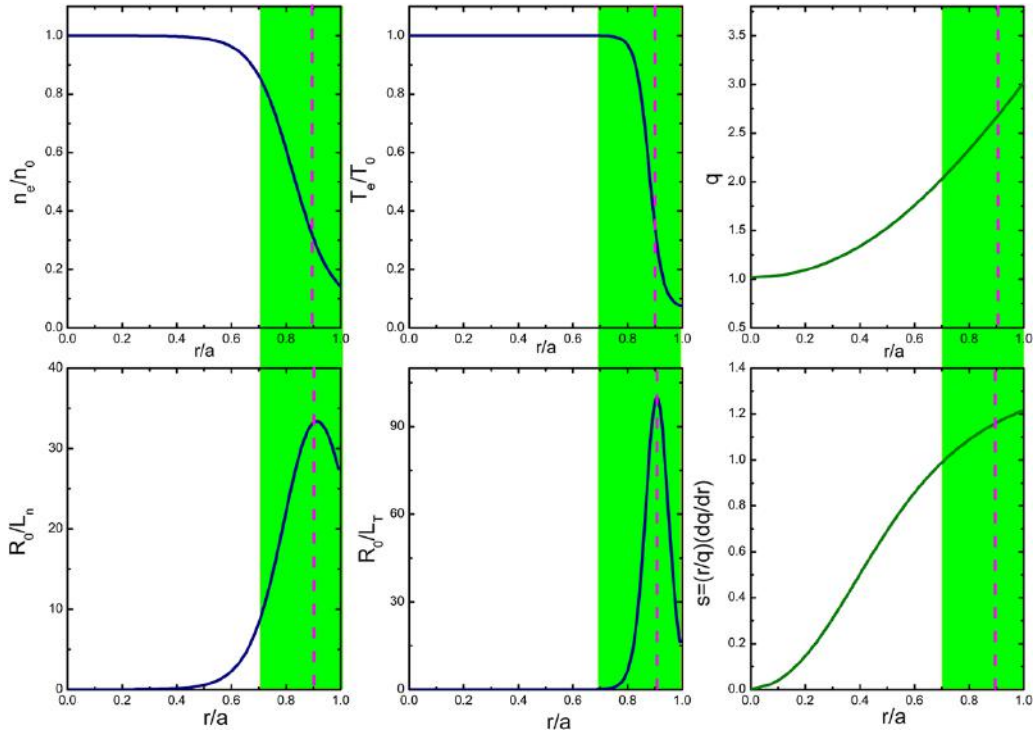

Figure 1. Normalized radial profiles of the electron density, temperature and safety factor in I-mode-like plasma. The vertical pink dashed line is indicates where the profile inverse scale lengths peak, and the green region is the simulation domain.

Table 1. The parameters of density, temperature gradient we used for the three different modes calculations.

	L-mode	I-mode-like	H-mode
R_0/L_n	33	33	100
R_0/L_T	33	100	100

3.1. Toroidal mode number variation

Figure 4 shows the mode frequency (ω) and growth rate (γ) as functions of the toroidal mode number n. The growth rate γ also increases when n increases, whereas the change of the frequency is more complicated. On one hand, with the increment of n, the frequency jumps from positive to negative, i.e. from electron drift direction to ion drift direction, which indicates there may be a transition for TEM to ITG in this process, or there exists an ITG mode propagating in electron drift direction. On the other hand, two modes coexist, and both propagate in the direction of ion drift direction when n is large enough. Therefore, these two modes are the ITG modes with large n.

In order to clarify whether the modes with lower n ($n \leqslant 15$) in figure 4 are TEM modes or ITG mode in electron direction, we performed a simulation with adiabatic electrons and found that the modes still existed and displayed typical unconventional structure in those circumstances. That means the ITG modes do dominate in these cases, and the physics of non-adiabatic electrons may have an influence on the results, but is not dominant here.

In order to see the modes structure for different n, the 2D mode structure of electrostatic potential (ϕ) of $n = 5$, $n = 15$, $n = 25$ and $n = 35$ at $t = 5000t_0$, are shown in figure 5. This figure clearly shows that the mode structure becomes narrower as the toroidal mode number increase. This phenomenon can be easily understood. Because from the global 2D drift wave model, the mode structure width depends on the inverse of $b = k_\theta^2 s^2 \omega_{\chi\chi} \vartheta_{kk}$, where s is the magnetic shear, $\omega_{\chi\chi} = \partial^2\omega/\partial\chi^2$,$\vartheta_{kk} = \partial^2\omega/\partial\vartheta^2$, the poloidal wave number k_θ is proportional to n, and parameter χ is an artificial coupling strength, default $\chi = 1$; whereas the model reduces to cylinder drift waves at $\chi = 0$. Therefore, higher n means narrower mode structure. On the other hand, solving the 2D eigenmode equation [42, 43], the mode amplitude factor $A(\theta_0)$ can be given as

$$A(\theta_0) = \exp\left[-\frac{nq'}{2}\left(\frac{\Omega_{\theta_0\theta_0}}{\Omega_{\chi\chi}}\right)^{1/2}(\theta_0 - \theta_m)^2\right] \qquad (7)$$

where $q' = dq/dr$, $A(\theta_0)$ has a width $\sim n^{-1/2}$. Generally speaking, the ITG in I-mode-like plasma has a conventional mode structure similar to that for the trapped electron mode (TEM) in L-mode plasma. However, in comparison with former TEM simulations [10], the characteristics of herringbone-like radial mode structures and multi modes coexisting, which will be investigated in detail in the following sections, are shown in an I-mode-like plasma.

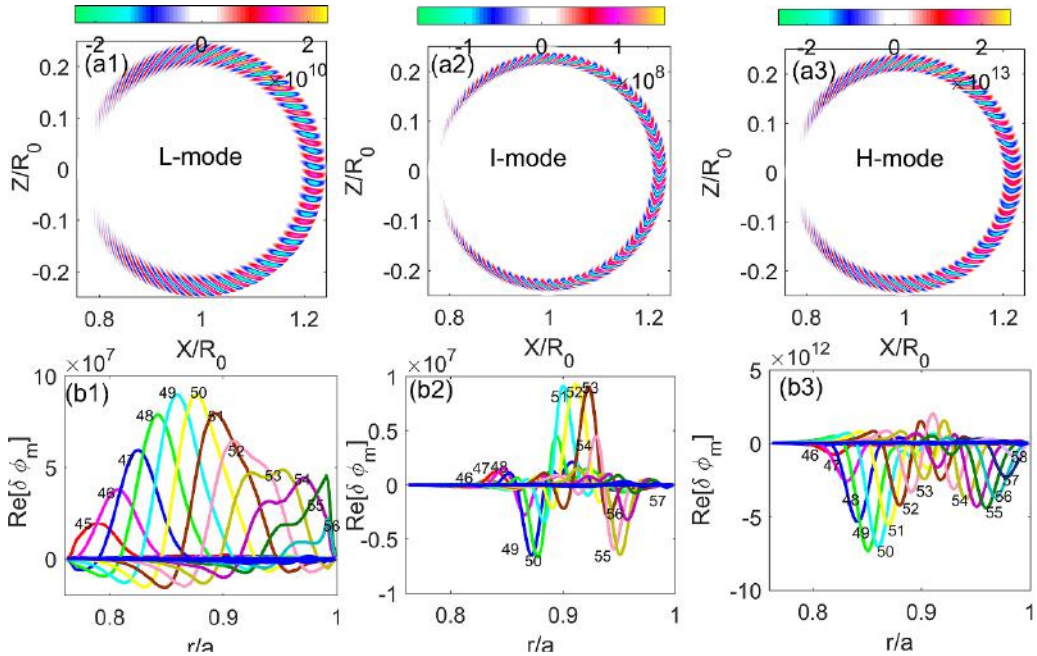

Figure 2. Structure of the electrostatic potential of the ITG instability under L-mode (a1), I-mode-like (b1) and H-mode (c1) in a poloidal cross section, and their corresponding parts of Fourier $\delta\phi_m$ at $t = 5000t_0$.

3.2. η effect

We now concentrate on the dependence of excitation of ITG modes on the value of η. Given in figure 6 is the mode growth rate (γ) and real frequency (ω_r) under different temperature gradient R_0/L_T with fixed $R_0/L_n = 33$. As shown in figure 6, the growth rate increases monotonically with low R_0/L_T. However when R_0/L_T is high, namely in I-mode-like plasmas, it does not change monotonically with R_0/L_T, and the amplitudes vary a little with the increment of R_0/L_T. In the scanning of R_0/L_T, we have discovered that the modes coexistence shows up with fixed $n = 20$. Especially at $R_0/L_T = 120$ and 140, there is a coexistence of three modes. Moreover, the existence of the third mode (the blue dotted line in figure 6(b)) seems decrease the frequency of the second mode (the pink line in figure 6(b)). The third mode could disappear if R_0/L_T is too high. And from the frequency spectrum we can find that the mode corresponding to the red line in figure 6 is the strongest mode. We can conclude that the temperature gradient, or η, is one of the critical factors for the excitation of the multiple ITG modes.

It should be noted that the instability in figure 6 is ITG modes. There are main three reasons that we judge this. First, since the collision between electrons is not considered in our model, the instability cannot be a resistive ballooning mode. Second, as we mentioned before, we performed a simulation with adiabatic electrons. We found that the modes still existed and displayed typical unconventional structure in those circumstances, indicating the mode is not TEM mode. Finally, because the instability mode we calculated is no longer a conventional mode, so the propagation direction cannot be used as a decisive criterion of the mode for the diagnosis of turbulence at the edge plasmas, that is, ITG may also be propagate in the electron diamagnetic direction, which can be seen from figure 9 in [44]. So even though the instability mode shown in the white area in figure 6(b) is in the electron propagation direction, it is still the ITG mode instability.

The mode structures of electrostatic potential in (X, Z) plane for ITG under different η are shown in figure 7. We can see that the conventional mode structure is displayed in I-mode-like plasmas. The η not only changes the mode width but also changes the mode radial peaking position. In addition, the herringbone-like radial mode structures still prevail under different η. The herringbone-like mode structures are usually found in experiments and simulations for Alfven eigenmode excited by energetic particle (EP) [45, 46]. The herringbone-like mode structures here can be well understood from the global theory. According to the previous global theory, a herringbone-like mode structure depends on the imaginary part of b. From figure 9 in [47], we can see that the sign of Im(b) determines the twisting direction, and the amplitude of Im(b) determines the width of the 'herringbone' structure. Therefore, smaller Δr, which determines the width of the steep profile region while a strong gradient of edge plasma means smaller Δr, leads to larger $\omega_{\chi\chi}$ and Im(b). This explains why the herringbone-like mode structures here shrink with higher η.

3.3. Multiple ITG modes

This part will further focus on the excitation of multiple ITG modes and its mode structure evolution in I-mode-like

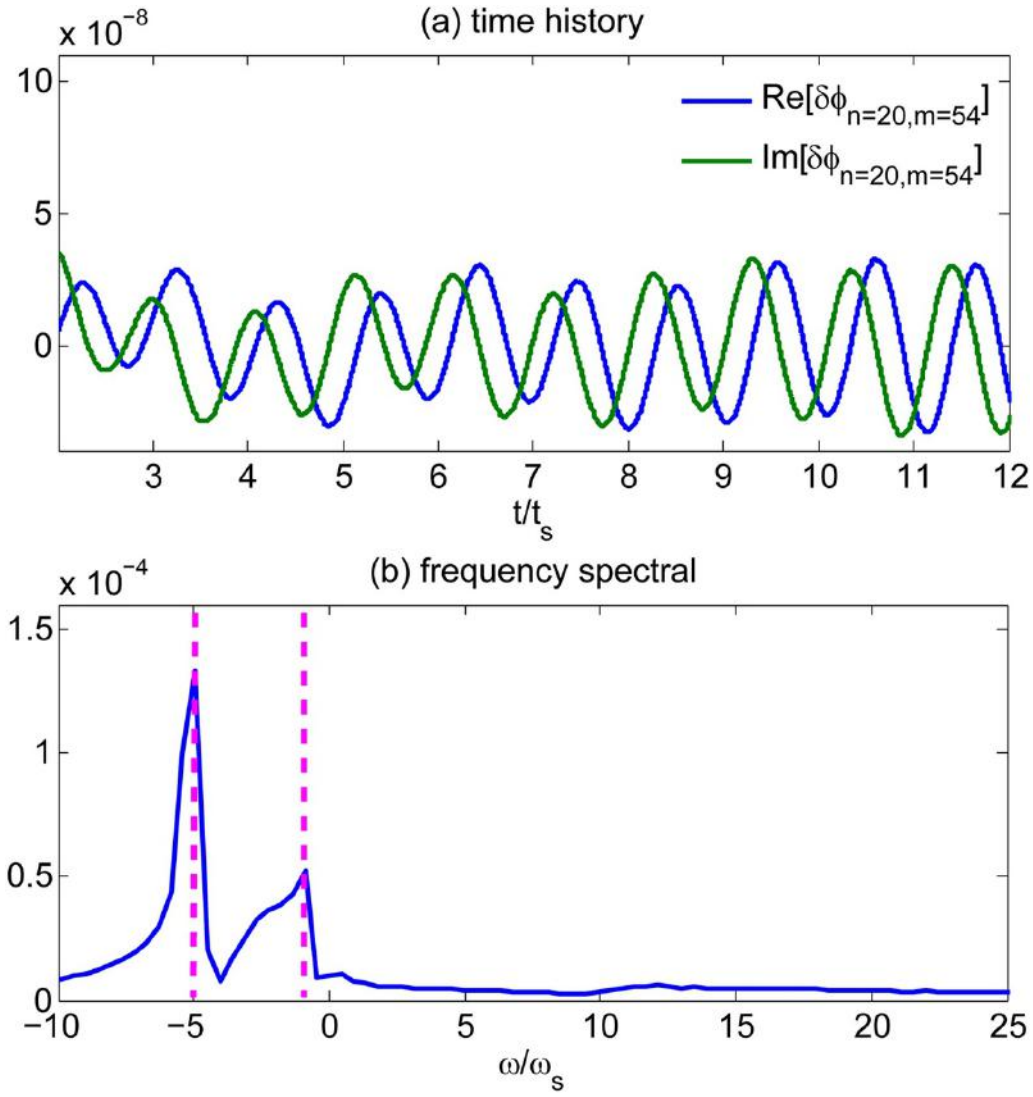

Figure 3. The time history (a) and frequency spectra (b) for the Fourier component ($n = 20$, $m = 54$) of electrostatic potential in the linear simulation with $R_0/L_n = 33$, and $R_0/L_T = 100$.

plasmas. It has been widely accepted that the steep pressure gradient (H-mode plasma) could lead to multi-modes coexisting [15], whereas our simulation indicates that the high temperature gradient is enough to excite multiple ITG modes. The evolutions of multiple ITG modes structure are shown in figure 8. $\eta = 2.4$ and 3.6 represent the cases of 2 and 3 modes co-existing situations, respectively. For the two modes co-existing, ITG modes with two radial peaks appear after about $t = 1000t_0$. Later on, the two modes peaking positions get closer and finally form a very regular herringbone-like mode structure. For the three modes co-existing, three branches of the eigenmode with different peaking position are excited. At $t = 3000t_0$, only two distinct peaking positions can be seen. Therefore, the evolution figure has shown that the growth rates of two branches overwhelm the third branch as time went by.

The poloidal mode structure of the electrostatic potential in figure 8 can be represented by the Fourier series $\delta\phi(r,\theta,\zeta,t) = e^{in\zeta - i\omega t}\sum_m \delta\phi_m(r)e^{-im\theta}$, where $\omega = \omega_r + i\gamma$ is the mode frequency. We proceed to examine the radial mode structures variation with time under different gradients, and the results are shown in figure 9. With $\eta = 2.4$, we find two branches of the eigenmode coexist at the initial linear stage, as shown in figure 9(a). Figure 9(c) indicates that one branch overwhelms the other after about $1000t_0$. In comparison with figure 9(b), the same results are shown for the situation with $\eta = 3.6$ as seen in figures 9(b) and (d), which apparently exhibit pictures of the three modes co-existing. These indicate that a clear sudden change of transport characteristics are presented with those radial Fourier components of $\delta\phi_m$ for the mode structures.

3.4. Effect of radial electric field in an I-mode-like plasma

We study the effect of radial electric field on the ITG mode in an I-mode-like plasmas. Firstly, the effects of rigid rotation,

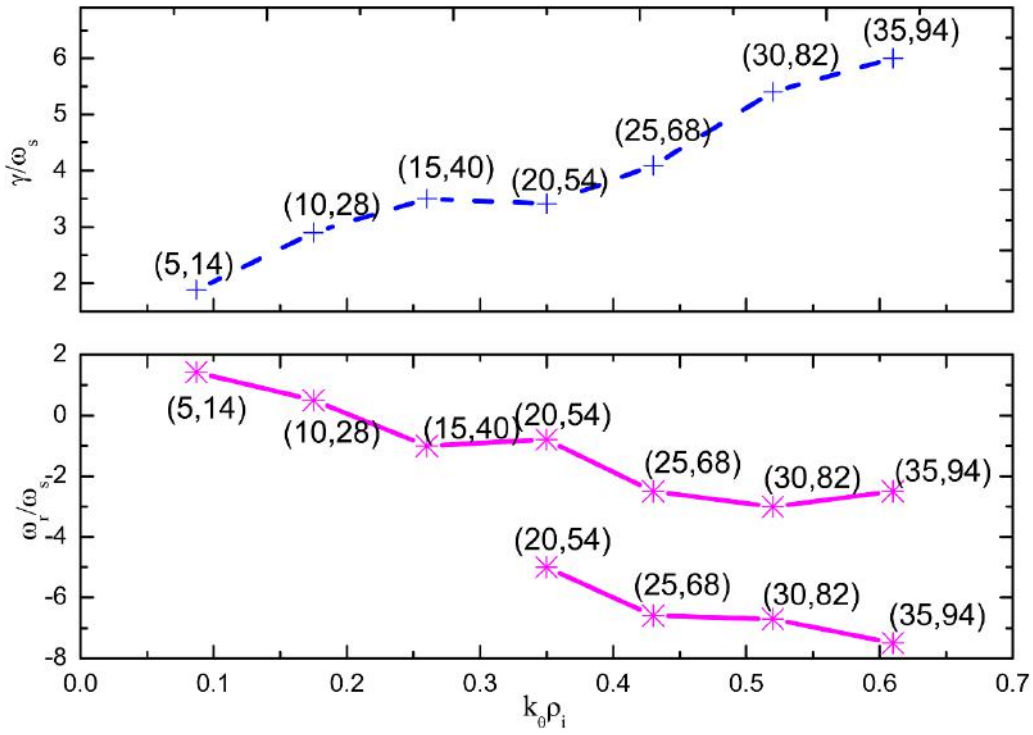

Figure 4. Mode growth rate (γ) and real frequency (ω_r) versus $k_\theta \rho_i$ with $R_0/L_n = 33$, and $R_0/L_T = 100$ in the I-mode-like plasma.

$\partial\phi_{eq}/\partial\psi_N =$ const., are tested, where ϕ_{eq} is the equilibrium electric potential and ψ_N is the poloidal magnetic flux normalized to the separatrix value. Without rotation, the ITG growth rate is $3.3\omega_s$, and the frequency is $-5.0\omega_s$. When considering the E_r rotation without shear, the ITG growth rate is $3.2\omega_s$ and the frequency changes to $-16.0\omega_s$. At this case, the doppler shift of frequency is $-10.2\omega_s$. Therefore, we have verified the implementation of radial electric field effects in GTC simulations. Secondly, we investigate the effect of the realistic radial electric field on the ITG modes in HL-2A pedestal. E_r induced by ∇P is considered only. We use the same initialization as in figure 3. Figures 10(a)–(c) illustrate the equilibrium pressure gradient, radial mode structure of the perturbed electrostatic potential without E_r, and with E_r, respectively. With E_r, the ITG growth rate is $2.5\omega_s$, and the real frequency is $-10.2\omega_s$. It is also demonstrated that adding E_r shear makes the radial mode structure shift to inner plasma region, and decreases the growth rate by 0.24, and increases the real frequency by 2.04.

Figures 11(a)–(c) give the 2D poloidal mode structures of the perturbed electrostatic potentials for the cases with sheared E_r, with rigid E_r, and without E_r, respectively. It can be seen that the effect of E_r shrinks the mode structure. This figure also demonstrates that the growth rate decreases when the E_r shear is added. Each snapshot in figure 11 is taken at the same time ($t = 5000t_0$) and each simulation uses the same initialization. Thus, the magnitudes from each figure can be compared with each other. What should be noted is that most our calculations did not consider the effect of E_r shear at present except in sections 3.4 and 3.5. However, E_r plays a role that cannot be ignored in ITG mode. Moreover, ∇P_i could be a dominant term contributing to E_r. Therefore the role of E_r shear given by ∇P_i needs to be considered in ITG research.

3.5. Nonlinear results

For nonlinear simulation, we first compare the turbulence characteristics in L-mode and I-mode-like plasma. Figure 12 shows the 2D nonlinear mode structures of the perturbed electrostatic potential at $t = 1800t_0$ and the ion heat conductivity for both L-mode and I-mode-like case. The heat conductivity χ_i is defined by the heat flux: $q_i = n_i\chi_i\nabla T_i \equiv \int dv^3(\frac{1}{2}m_iv^2 - \frac{3}{2}T_j)\delta v_E\delta f_i$, with v_E the $E \times B$ drift caused by turbulence. It can be seen from figure 12 that the mode structure is rather chaotic due to mode-mode coupling in the nonlinear phase, regardless of the L-mode or I-mode-like. There is no clear and regular mode structure in the calculations of the two modes. The herringbone mode structure is no longer obvious in I-mode-like plasmas. It can be seen in figure 12(c) that the heat conductivity of ions under L-mode is much greater than that under I-mode-like plasma. Therefore, this shows that there is stronger transport in L-mode, that is, it verifies that the plasma has a better confinement level in an I-mode-like plasma. It should be noted that the results presented in figure 12 include an equilibrium rigid E_r. We also calculated the influence of a sheared E_r on ITG turbulence, and the results show that the contribution of the stronger equilibrium $E \times B$ shear flow due to the steeper pressure gradient to the reduction of χ_i can reach 30% in the I-mode case relative to that of the L-mode. In addition, rigid E_r has very mild effect on the nonlinear results, and has little effect on energy transport.

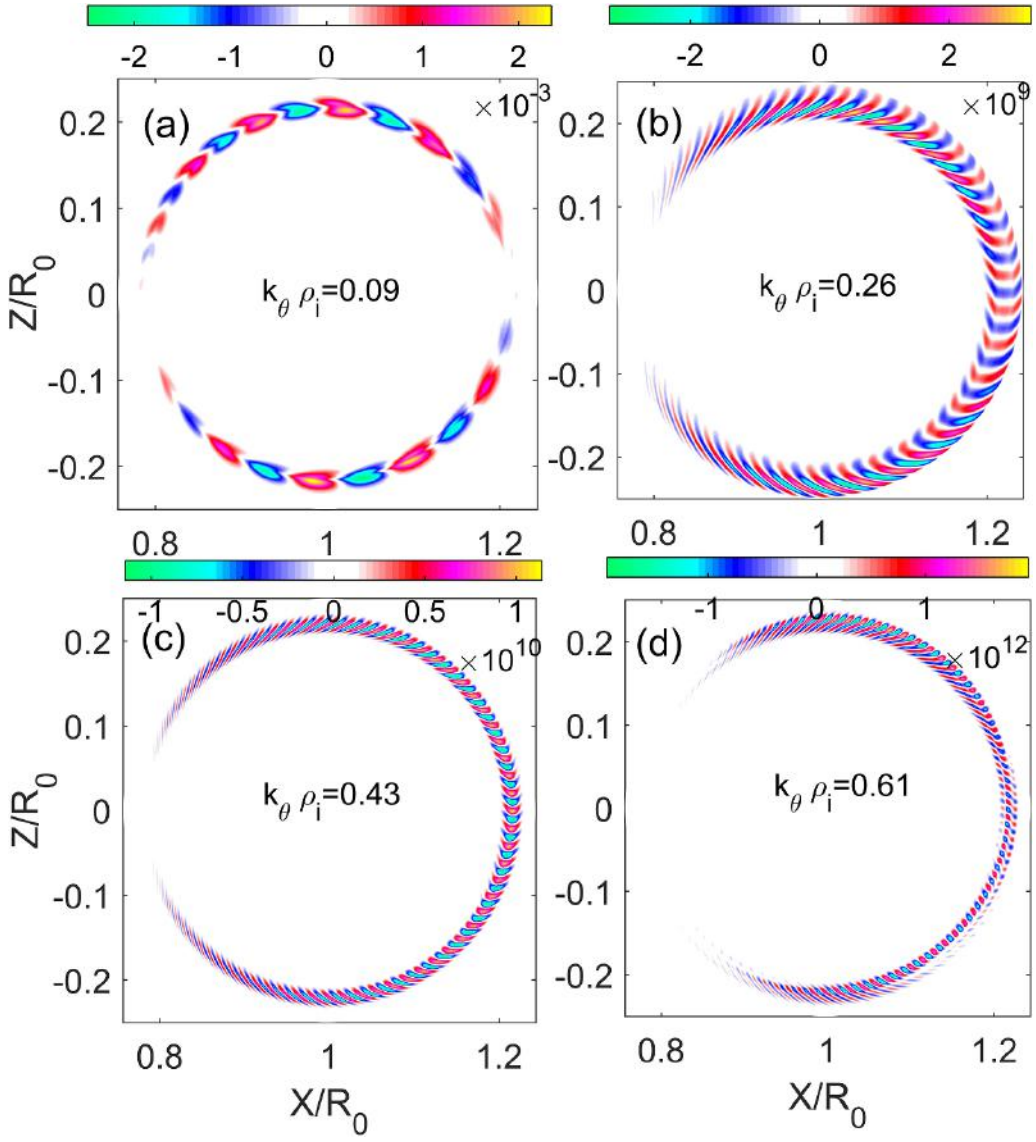

Figure 5. The 2D mode structure of electrostatic potential (ϕ) of $k_\theta \rho_i = 0.09$, 0.26, 0.43 and 0.61, respectively.

In the nonlinear simulation for plasmas with medium density and steep temperature gradient, we found that the larger the gradient, the greater the growth rate, but the smaller the transport coefficient. This trend is completely different from that under weak gradients. The greater the gradient, the greater the transport coefficient is with weak gradients [48]. This phenomenon can be explained as follows. The transport coefficient across the magnetic field can be estimated by: $D = l_c/\tau_c$, where the correlation length l_c is equivalent to the free path, and the correlation time τ_c is similar to the collision time. We noticed that as the gradient becomes larger, although the correlation length l_c may become smaller, the growth rate is greater, so the correlation time τ_c may also be shorter. The transport coefficient does not necessarily become smaller as the gradient becomes larger. We also need to see which of the growth rate and the mode structure has the greatest effect on the change in transport. From figure 12, it can be seen that the mode structure is much more chaotic when the gradient is large, and the correlation length is small; while the gradient is small, the radial flow structure is more obvious, and the correlation length is large. This result shows that the decrease in transport caused by the decrease in correlation length can indeed suppress the increase in transport caused by the decrease in correlation time, which leads to a decrease in the overall transport coefficient.

The generation of the GAM and its interaction with the turbulence are also investigated in the nonlinear simulation. Generally speaking, zonal flow plays an important role in regulation of turbulence and saturation level of turbulence. At the edge of the plasma, the zonal flow mainly exists in the form of GAM, which coexists with the near zero-frequency zonal flows [49, 50]. This is because the safety factor is relatively large at plasma edge region, causing the damping of the GAM to be smaller than that of the low-frequency zonal flow. This can be seen from the expression of GAM Landau damping rate:

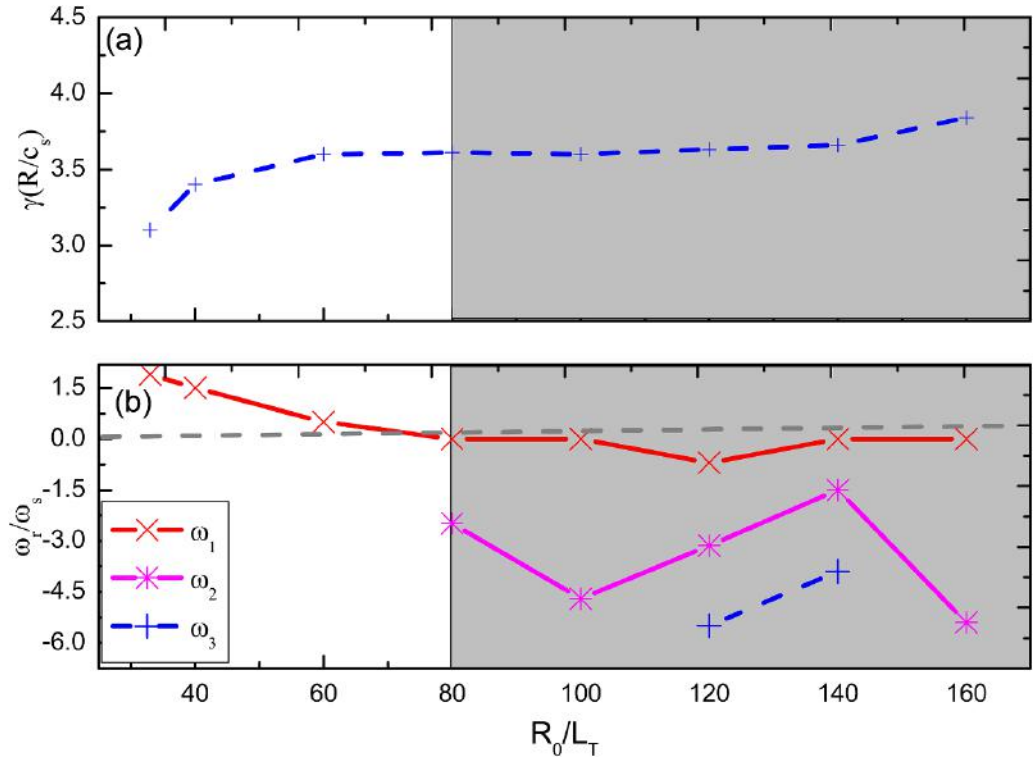

Figure 6. The mode growth rate (γ) (a) and real frequency (ω_r) (b) versus the temperature gradient R_0/L_T. The gray region corresponds to the tokamak plasma with medium density and steep temperature gradient.

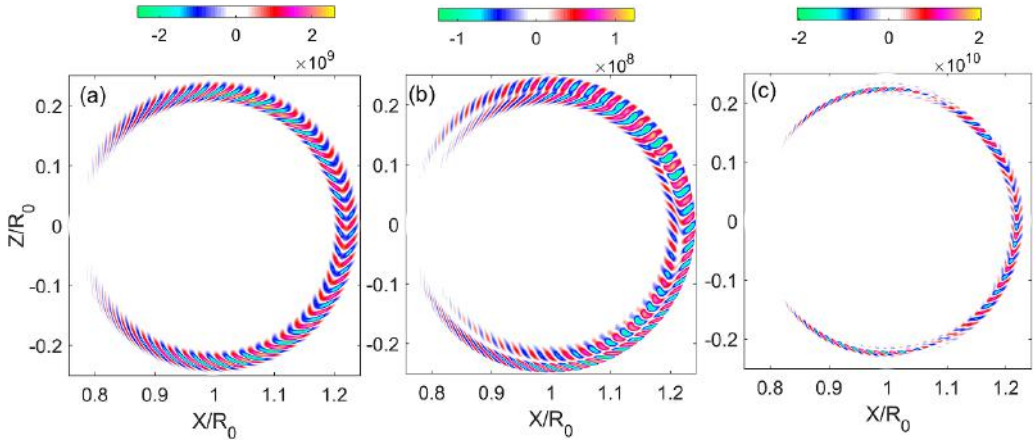

Figure 7. Mode structures of electrostatic potential in (X), (Z) plane for ITG observed in GTC simulation using HL-2A tokamak I-mode-like plasma parameter, where (a) $\eta = 2.4$, (b) $\eta = 3.6$, and (c) $\eta = 4.8$. The $R_0/L_n = 33$ in the three cases.

$$\gamma_{\rm GAM} = \frac{\pi^{1/2}}{2}\frac{v_i}{R}\frac{(R\omega_{\rm GAM}/v_i)^6}{7/4+\tau}q^5\exp\left[-\left(\frac{qR\omega_{\rm GAM}}{v_i}\right)^2\right]. \quad (8)$$

Here, $\tau = T_e/T_i$, v_i is the thermal velocity of the ions. The frequency of GAM can be calculated by the following formula through linear theory:

$$\omega^2_{\rm GAM} = (7/4+\tau)\frac{v_i^2}{R^2}\left[1+\frac{46+23\tau+8\tau^2}{(7/4+\tau)^2}q^2\right]. \quad (9)$$

We have also performed frequency spectrum analysis on E_r structure and turbulence. The results show that the frequency of GAM E_r structure is about 3 KHz, and the frequency of turbulence is about 20 KHz, which means that $\omega_{\rm GAM} < \omega_{\rm Tur}$ is satisfied. This result is consistent with the results in the earlier analytical analysis [51].

Figure 13 presents the time evolution of the flux surface averaged turbulence intensity and zonal flow electric field on a flux surface, as well as the electron particle flux (both in L-mode and I-mode-like plasmas) and energy flux. From figures 13(a) and (b), we could see the periodic modulation effect of GAM on turbulence and transport. The specific process is: turbulence first grows linearly, and then drives GAM in the nonlinear phase. The growth of GAM has a time lag

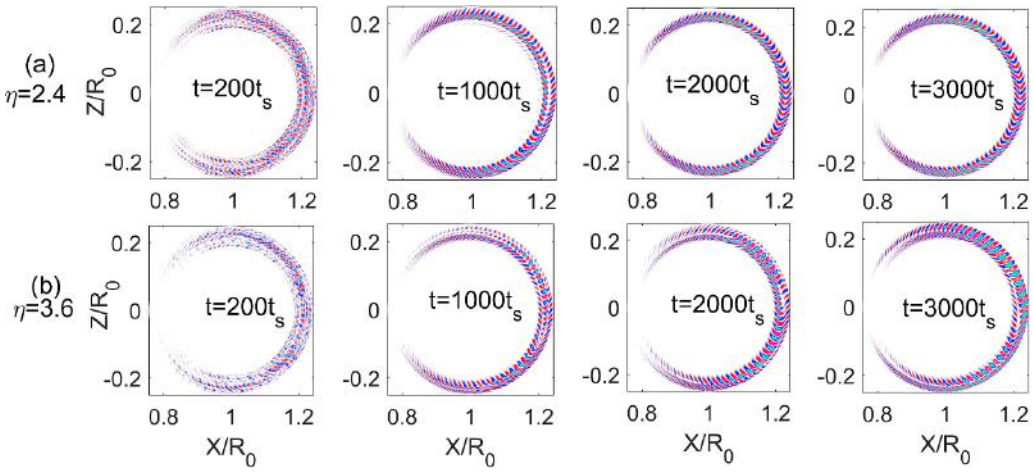

Figure 8. Time slices of 2D mode structure of electrostatic potential ($\delta\phi$) of simulations with two different values of η, i.e. (a) $\eta = 2.4$, (b) $\eta = 3.6$, representing the cases of 2 and 3 modes co-existing situations, respectively. The four panel (from the left to the right) are corresponding to the time $t = 200$, 1000, 2000, $3000t_0$.

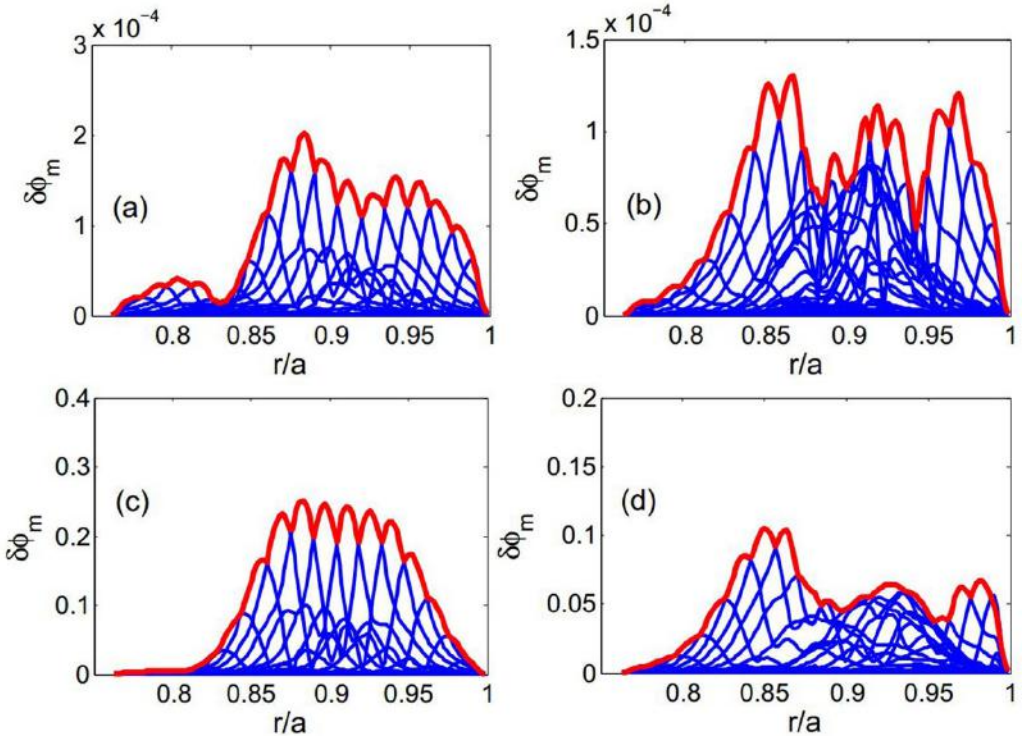

Figure 9. The Fourier part of $\delta\phi_m$ for the mode structures in figure 8, (a) $\eta = 2.4$, $t = 1000t_0$, (b) $\eta = 3.6$, $t = 1000t_0$, (c) $\eta = 2.4$, $t = 2000t_0$, (d) $\eta = 3.6$, $t = 2000t_0$. The red lines are envelopes of the lines with different m modes.

behind the growth of turbulence, and leads to the decrease of turbulence. This process is repeated in the non-linear phase. The characteristics of turbulence and GAM show a predator-prey relationship. We can also calculate the frequency of the GAM through the oscillation of the electric field of the GAM at a fixed position. As shown in figure 13(b), the frequency of GAM given by the GTC simulation result is $0.6c_s/R_0 \approx 3$ KHz, which is approximately equal to $0.41v_i/R_0$ and is basically the same as the theoretical result $0.5v_i/R_0$ calculated by formula (9). This result shows that this oscillation is the GAM oscillation. Figures 13(c) and (d) showed the electron particle flux and energy flux. It can be seen that the energy flows of electrons and electron particle flux have a relatively consistent growth process. Figure 13(c) also demonstrates that the particle flux in the I-mode-like plasma is ultimately greater than the particle flux in the L-mode. This confirms that the I-mode has a strong particle transport, and this feature is beneficial to impurities exhausting for fusion plasma.

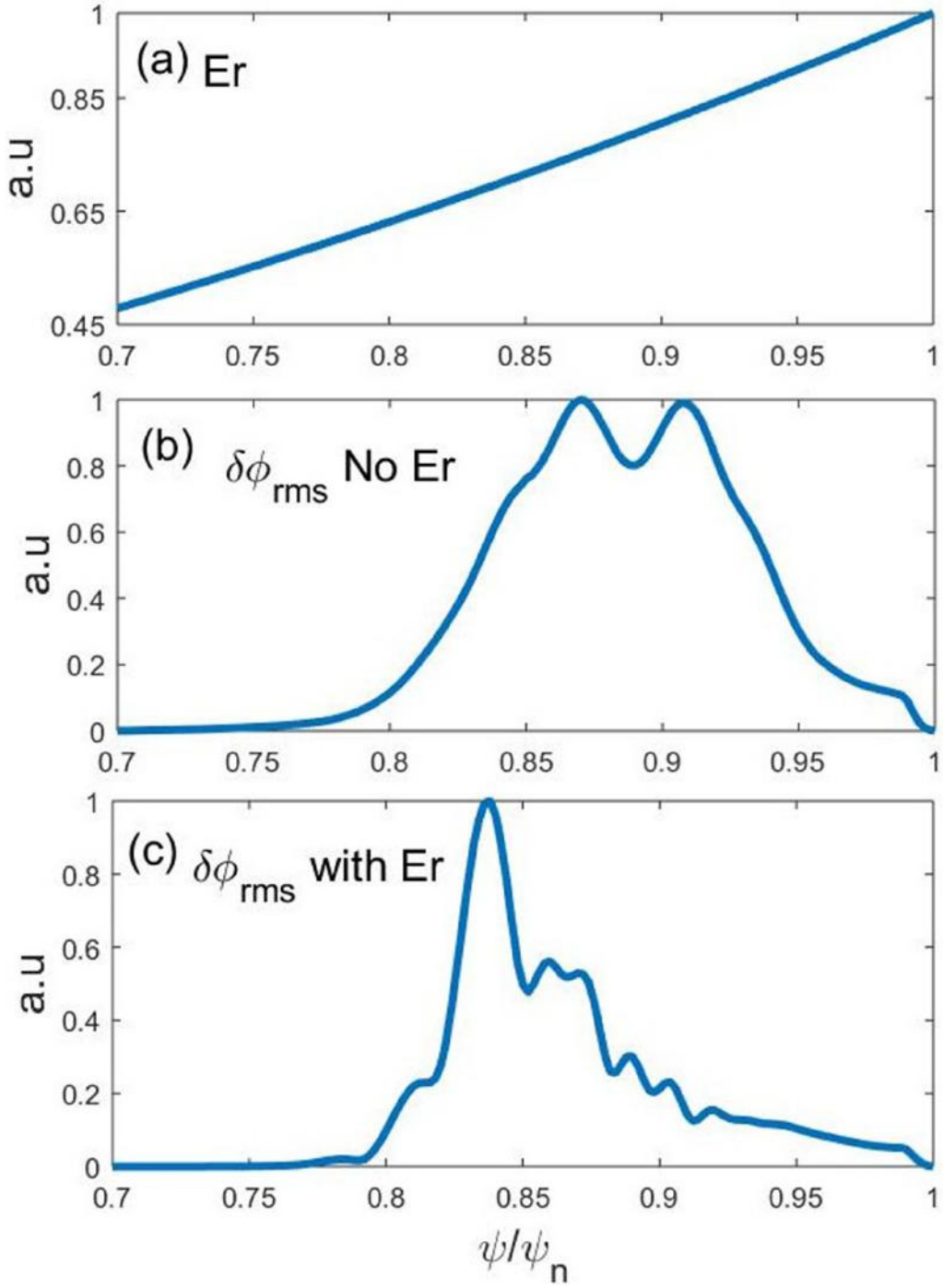

Figure 10. GTC linear electrostatic simulations of HL-2A pedestal. (a) The equilibrium pressure gradient, radial mode structure of the perturbed electrostatic potential (b) without E_r, and (c) with E_r.

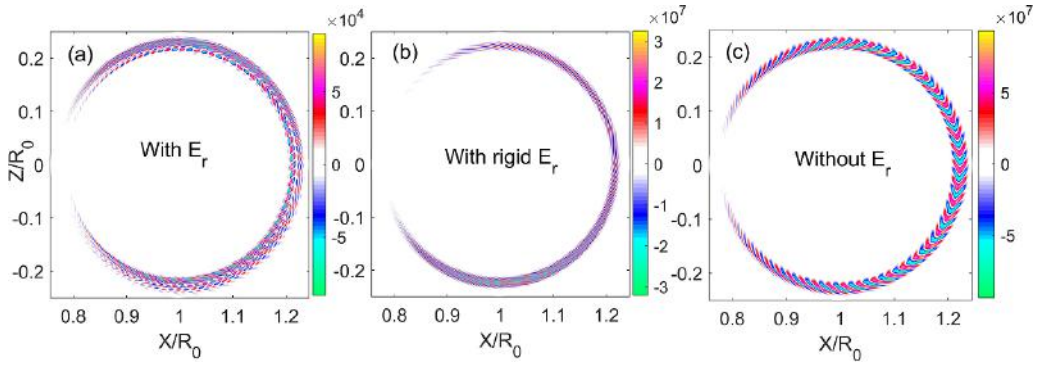

Figure 11. 2D linear mode structures of the perturbed electrostatic potential for the cases: (a) with E_r, (b) with E_r corresponding to rigid rotation, and (c) without E_r. Each snapshot is taken at the same physical time ($t = 5000t_0$) and each simulation uses the same initialization as in figure 1.

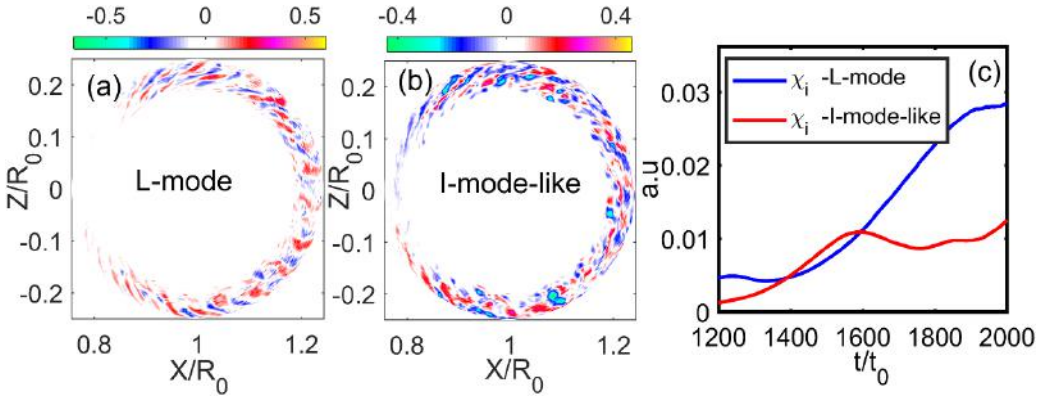

Figure 12. (a), (b) 2D nonlinear mode structures of the perturbed electrostatic potential at $t = 1800t_0$ for the nonlinear simulations. (c) ion heat conductivity for both L-mode and I-mode-like case.

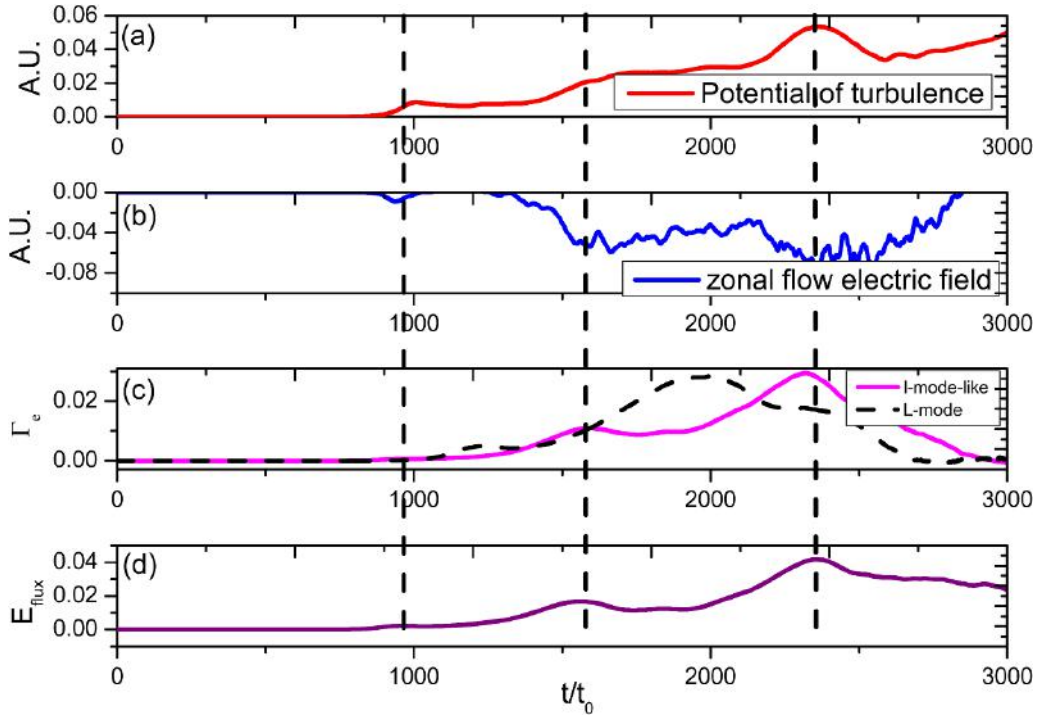

Figure 13. (a), (b) The time evolution of the flux surface averaged turbulence intensity and electric field of zonal flow on one flux surface; (c), (d) the electron particle flux and energy flux.

4. Conclusions

In this paper, we systematically present simulation results on global ITG modes in TBs of I-mode-like plasmas with code GTC for the first time. The simulations use annulus geometry and concentrate on the transport barriers with HL-2A parameters. It is found that the conventional ion temperature gradient modes are dominant in I-mode-like plasmas. The growth rate of ITG mode increases and its mode structure shrinks with increasing toroidal mode number. These results are in agreement with the global 2D drift wave model.

In I-mode-like plasmas, the ITG modes with herringbone-like mode structures can be excited, and the mode width shrinks with the increment of the ratio of gradients density to temperature. This result is consistent with the global analytical prediction. In addition, the simulation results indicate that multiple ITG modes are induced with a high temperature gradient. The effect of radial electric field on drift wave in the I-mode-like plasma is also investigated. It shows that E_r corresponding to rigid rotation only changes the frequency of ITG mode, while the E_r shear decreases the mode growth rates while increases the real frequency of ITG modes. Nonlinear calculations find that the frequency of GAM given by the GTC is basically the same as the theoretical result and we could also see that the periodic modulation effect of GAM on turbulence and transport. These features are important to the exploration of the transition of confinement regimes and transport in transport barriers.

It should be noted that the linear herringbone mode structure in our calculations implies that the turbulent transport level decrease with the increase of the pressure gradient, that is, the turbulent transport level is lower under a strong gradient. This is consistent with I-mode-like turbulence in the nonlinear calculations, and it also confirms that the I-mode-like plasma has better confinement performance than the L-mode. Besides, we have not carried out I-mode experiments on HL-2A up to now, so it is temporarily impossible to compare the simulated transport level with the experiment, but this will be carried out in the future with experiments.

The present work is a starting point to understand the micro-turbulence in I-mode plasmas. Some assumptions have made in the present study, such as considering the electrostatic perturbations only, and not considering the influence of the scrape-off layer. However, this is our first step that focuses on electrostatic perturbations under strong temperature gradients. Electromagnetic perturbations may be important in the pedestals, and the effect of scrape-off layer may have an impact on the turbulence structure in the pedestal. These are the physical issues we will take into account step by step. Future works will also include validation of drift wave in realistic I-mode plasma configuration, nonlinear simulation to clarify the interaction between zonal flow, zonal field, and the low-frequency geodesic acoustic mode. Electromagnetic simulations will also be necessary in order to find whether electrostatic or electromagnetic modes are dominant in the edge of I-mode plasmas. All of those will contribute to the understanding of the transport in the edge plasmas.

Data availability statement

The data generated and/or analysed during the current study are not publicly available for legal/ethical reasons but are available from the corresponding author on reasonable request.

Acknowledgments

The authors would like to thank X Wang at HIT, Min Xu, L W Yan, J Q Li, J Cheng and Jun Wang at SWIP, Youjun Hu at ASIPP for fruitful discussions. This work is supported by the National Key *R&D* Program of China (Nos. 2018YFE0303102 and 2017YFE0301702), NSFC (Nos. 11905109 and 11947238), and the U.S. Department of Energy, Office of Science, Office of Advanced Scientific Computing Research and Office of Fusion Energy Sciences, and the Scientific Discovery through Advanced Computing (SciDAC) program under Award No. DE-SC0018270 (SciDAC ISEP Center). This work used resources of the Oak Ridge Leadership Computing Facility at the Oak Ridge National Laboratory (DOE Contract No. DE-AC05-00OR22725) and the National Energy Research Scientific Computing Center (DOE Contract No. DE-AC02-05CH11231). We also thank to the Center for Computational Science and Engineering of Southern University of Science and Technology.

ORCID iDs

Jingchun Li https://orcid.org/0000-0001-9918-8880
Huasheng Xie https://orcid.org/0000-0001-9204-135X

References

[1] Horton W 1999 *Rev. Mod. Phys.* **71** 735
[2] Wagner F *et al* 1982 *Phys. Rev. Lett.* **49** 1408
[3] Lin Z, Hahm T S, Lee W W, Tang W M and White R B 1998 *Science* **281** 1835
[4] Hasegawa A 1969 *Phys. Fluids* **12** 2642
[5] Dong J Q, Horton W and Kim J Y 1992 *Phys. Fluids* **B4** 1867
[6] Dong J Q, Horton W and Kishimoto Y 2001 *Phys. Plasmas* **8** 167
[7] Li J C, Liu S F, Kong W, Guo S C and Dong J Q 2019 *Europhys. Lett.* **127** 45002
[8] Hatch D R *et al* 2011 *Phys. Plasmas* **18** 055706
[9] Hatch D R *et al* 2011 *Phys. Rev. Lett.* **106** 115003
[10] Liu F, Lin Z, Dong J Q and Zhao K J 2010 *Phys. Plasmas* **17** 112318
[11] Dong J Q and Horton W 1995 *Phys. Plasmas* **2** 3412
[12] Jingchun Li, Dong J and Liu S 2020 *Plasma Sci. Technol.* **22** 055101
[13] Jia M X *et al* 2021 *Nucl. Fusion* **61** 046033
[14] Fulton D P, Lin Z, Holod I and Xiao Y 2014 *Phys. Plasmas* **21** 042110
[15] Xie H S and Xiao Y 2015 *Phys. Plasmas* **22** 090703
[16] Xie H S, Xiao Y and Lin Z 2017 *Phys. Rev. Lett.* **118** 095001
[17] Watanabe T-H, Sugama H and Ferrando-Margalet S *et al* 2007 *Nucl. Fusion* **47** 1383

[18] Chang C S, Ku S, Diamond P H, Lin Z, Parker S, Hahm T S and Samatova N 2009 *Phys. Plasmas* **16** 056108
[19] Rameswar Singh S Ganesh B, R and Jenko F 2014 *Phys. Plasmas* **21** 032115
[20] Whyte D G *et al* 2010 *Nucl. Fusion* **50** 105005
[21] Hubbard A E *et al* 2017 *Nucl. Fusion* **57** 126039
[22] Ryter F *et al* 2017 *Nucl. Fusion* **57** 016004
[23] Feng X *et al* 2019 *Nucl. Fusion* **59** 096025
[24] Mikkelsen D R, Howard N T, White A E and Creely A J 2018 *Phys. Plasmas* **25** 042505
[25] Stimmel K *et al* 2019 *Phys. Plasmas* **26** 122504
[26] Yang H, Zhou T and Xiao Y 2021 Gyrokinetic simulation of turbulent transport for I-mode edge plasmas *Nucl. Fusion* **61** 056006
[27] Lin Z, Tang W M and Lee W W 1995 *Phys. Plasmas* **2** 2975
[28] Lin Z, Hahm T S, Lee W W, Tang W M and Diamond P H 1999 *Phys. Rev. Lett.* **83** 3645
[29] Hahm T S 1988 *Phys. Fluids* **31** 2670
[30] Lee W W 1987 *J. Comput. Phys.* **72** 243
[31] Parker S E and Lee W W 1993 *Phys. Fluids* B **5** 77
[32] Dimits A M and Lee W W 1993 *J. Comput. Phys.* **107** 309
[33] Xu X Q 2008 *Phys. Rev.* E **78** 016406
[34] Holod I and Lin Z 2013 *Phys. Plasmas* **20** 032309
[35] Hager R *et al* 2020 *Phys. Plasmas* **27** 062301
[36] Lin Z, Nishimura Y, Xiao Y, Holod I, Zhang W L and Chen L 2007 *Plasma Phys. Control. Fusion* **49** B163
[37] Li J C, Xiao C J, Lin Z H and Wang K J 2017 *Phys. Plasmas* **24** 082508
[38] Yao Y, Lin Z, Dong J *et al* 2021 *Phys. Lett. A* **417** 127681
[39] Li J, Xiao C, Lin Z, Liu D, Ji X and Wang X 2020 *Phys. Plasmas* **27** 042507
[40] Liao X, Lin Z, Holod I, Li B and Sun G Y 2016 *Phys. Plasmas* **23** 122305
[41] Hahm T S 1996 *Phys. Plasmas* **3** 4658
[42] Hahm T S *et al* 2009 *Phys. Plasmas* **16** 022305
[43] Dickinson D, Roach C M, Skipp J M and Wilson H R 2014 *Phys. Plasmas* **21** 010702
[44] Xie H S *et al* 2017 *Phys. Plasmas* **24** 072106
[45] Deng W, Lin Z, Holod I, Wang X, Xiao Y and Zhang W 2010 *Phys. Plasmas* **17** 112504
[46] Wang X *et al* 2012 *Phys. Rev.* E **86** 045401(R)
[47] Xie H S *et al* 2016 *Phys. Plasmas* **23** 082513
[48] Dimits A M *et al* 2000 *Phys. Plasmas* **7** 969
[49] Cziegler I *et al* 2013 *Phys. Plasmas* **20** 055904
[50] Manz P *et al* 2015 *Nucl. Fusion* **55** 083004
[51] Hahm T S *et al* 1999 *Phys. Plasmas* **6** 922